



# Effect of photo-induced charge separated state lifetimes in donor-acceptor1-acceptor2 organic ambipolar semiconductors on their photovoltaic performances



Tianyang Wang<sup>a, b, \*</sup>, Haiya Sun<sup>a, b</sup>, Linli Zhang<sup>a, b</sup>, Nathan D. Colley<sup>c</sup>, Chelsea N. Bridgmohan<sup>c</sup>, Dongzhi Liu<sup>a, d</sup>, Wenping Hu<sup>b, e</sup>, Wei Li<sup>a, d</sup>, Xueqin Zhou<sup>a, b, d, \*\*</sup>, Lichang Wang<sup>a, b, c, \*\*\*</sup>

<sup>a</sup> School of Chemical Engineering and Technology, Tianjin University, Tianjin, 300354, China

<sup>b</sup> Collaborative Innovation Center of Chemical Science and Engineering, Tianjin, 300072, China

<sup>c</sup> Department of Chemistry and Biochemistry and the Materials Technology Center, Southern Illinois University Carbondale, IL 62901, United States

<sup>d</sup> Tianjin Engineering Research Center of Functional Fine Chemicals, Tianjin, 300354, China

<sup>e</sup> School of Science, Tianjin University, Tianjin, 300354, China

## ARTICLE INFO

### Article history:

Received 22 December 2016

Received in revised form

28 December 2016

Accepted 28 December 2016

Available online 30 December 2016

### Keywords:

Donor-acceptor1-acceptor2 system

s-triazine

Fullerene

Photo-induced electron transfer

Single-layer organic solar cell

Photovoltaic property

## ABSTRACT

A newly ambipolar organic semiconductor with styrene based indoline derivative (YD) as the electron donor (D), s-triazine group (TRC) as the electron acceptor (A<sub>1</sub>), and fullerene derivative (NMF) as the second electron acceptor (A<sub>2</sub>) has been synthesized and characterized, which had a charge-separated state of 7.9 μs, corresponding to a 37 fold increase in comparison with the 215 ns lifetime of the D-A<sub>1</sub> precursor. Here we compared photovoltaic properties of YD-TRC-NMF with those of other four D-TRC-A<sub>2</sub> systems, which replaced indoline with triphenylamine (MTPA) and fullerene with perylene bisimide or anthraquinone (AEAQ), indicating that long-lived CS states are playing an important role in promoting photoelectric conversion in YD-TRC-AEAQ (or NMF) and MTPA-TRC-AEAQ, in which the short-circuit current and photoelectric conversion efficiency were significantly improved in comparison with YD-TRC and MTPA-TRC, respectively, due to triplet states of A<sub>2</sub> being higher than charge-separated states. This proves that a general D-A<sub>1</sub>-A<sub>2</sub> architecture can become a reasonable materials design strategy for photovoltaics.

© 2016 Elsevier Ltd. All rights reserved.

## 1. Introduction

Natural photosynthesis, the most efficient process of converting sunlight into electrical or chemical energy, is of great interest to researchers focused on energy conversion and utilization. In a natural photosynthetic system, long-lived charge-separated (CS) states are formed via multistep electron transfers upon light

absorption and are believed to be the key for the subsequent chemical reactions [1–3]. Great efforts have been made to design dyes in which long-lived CS states are attained through photo-induced electron transfer [4–9]. In several of the artificial photosynthetic complexes, photo-induced CS states have reached the lifetimes of 380 ms to 2 h that are comparable to, or even longer than those in nature photosynthetic systems [5,7]. It is recognized that materials with long-lived CS states may improve the performance of organic solar cells (OSCs) [10–13]. Actually, generation of CS states with suitable lifetimes is critical in the formation of photocurrents for solar cells [14–17], that means the study of photoinduced charge separation processes and investigation of their essential role in improving the efficiency of solar cell devices should be required in depth. However, only a few publications have focused on the application of long-lived CS organic compounds to OSCs. It is important to perform systematic studies to establish a relationship between the lifetimes of CS states and the photovoltaic

\* Corresponding author. School of Chemical Engineering and Technology, Tianjin University, Tianjin, 300354, China.

\*\* Corresponding author. School of Chemical Engineering and Technology, Tianjin University, Tianjin, 300354, China.

\*\*\* Corresponding author. Department of Chemistry and Biochemistry and the Materials Technology Center, Southern Illinois University Carbondale, IL 62901, United States.

E-mail addresses: [tianyangwang@tju.edu.cn](mailto:tianyangwang@tju.edu.cn) (T. Wang), [zhouxueqin@tju.edu.cn](mailto:zhouxueqin@tju.edu.cn) (X. Zhou), [lwang@chem.siu.edu](mailto:lwang@chem.siu.edu) (L. Wang).

performance of OSCs. This contains two levels of work: 1) Design and construction of organic materials which had long-lived CS states; 2) Select the appropriate structure of OSCs device to investigate the effect of long-lived CS states of the material effectively.

Photo-induced CS were discovered in organic systems containing donor (D) and acceptor (A) moieties via photo-induced intramolecular electron transfer. This result suggests that D and A determine the driving force of electron transfer [18–20] while the distance, spatial orientation, and flexibility between D and A have a marked impact on the rate of photo-induced electron transfer and the efficiency of generating CS species and lifetimes of CS states. Photo-induced CS states can also be created by photo-induced hole transfer when the acceptor moiety is initially photo-excited [19]. That means that ambipolar organic semiconductors, which include both photo-induced electron and hole transfers, can form CS states effectively because of the synergistic combination of above two transfers [21–28]. Using a D-A<sub>1</sub>-A<sub>2</sub> strategy, we reported an ambipolar organic semiconductor MTPA-TRC-AEAQ using *s*-triazine (TRC) as the first acceptor to connect the donor styrene based triphenylamine (MTPA) with anthraquinone (AEAQ) as the second acceptor, which had been proven to be a good linker to promote the photo-induced electron transfer and increase the light-stability for MTPA-TRC-AEAQ [29,30]. Upon the absorption of photons, the CS states in the organic semiconductor MTPA-TRC-AEAQ was elongated to 650 ns, more than eight-fold compared to those in the D-A<sub>1</sub> precursor MTPA-TRC (80 ns). MTPA-TRC exhibits similarly low photovoltaic characteristics in the single layer OSCs with common organic semiconductors such as phthalocyanine, poly(phenylenevinylene) and triarylamine derivatives [12,31–33], of which the efficiency has been improved to greater than 6% and can even exceed 10% by the combined application of other semiconductors and the proper design of solar cell structures [12,34–39]. Importantly, the single layer OSCs constructed using MTPA-TRC-AEAQ were found to be significantly more efficient than those using MTPA-TRC [29], indicating that single layer OSCs had been proven to be the highly effective cell structure reflecting the effect of long-lived CS states of organic materials directly. That was why we chose single-layer OSC structure in this paper, although its photoelectric conversion efficiency was relatively low in various literature [12,31–33,38,40–42].

Encouraged by these results, we obtained a new ambipolar organic semiconductor YD-TRC-AEAQ by substitution of MTPA for an indoline derivative (YD) which has been reported to be a more effective donor [29,43,44]. The lifetime of CS states reached 1.14 μs for YD-TRC-AEAQ [44]. Further studies suggest that charge separation efficiency and lifetime of CS states may be controlled by changing the donor and second acceptor of MTPA-TRC-AEAQ [29,43–45]. The aforementioned ambipolar organic semiconductors have cascade energy levels and similar photophysical processes to generate photo-induced CS states. Therefore, it is possible and significant to relate their CS states to the photovoltaic performance of single layer OSC devices, and reveals the advantage of introducing the acceptor<sub>2</sub> to D-A<sub>1</sub> system to form the D-A<sub>1</sub>-A<sub>2</sub> architecture in the research perspective of photovoltaic characteristics.

To systematically study the solar cell performance of these promising materials and to establish correlation between the lifetime of charge separation and cell efficiency, more systems are required. Therefore, we have synthesized a new ambipolar organic semiconductor, YD-TRC-NMF, introducing a fullerene derivative (NMF) as the second acceptor (Figs. S1–S2 of Electronic Supplementary Information (ESI)) to the reported D-A<sub>1</sub> system YD-TRC [43,44]. We investigated its photophysical properties by absorption and emission spectra, which showed that YD-TRC-NMF can

generate the CS state with lifetime of 7.9 μs. Then, we fabricated single layer OSCs devices with all of the above D-A<sub>1</sub>-A<sub>2</sub> systems with their D-A<sub>1</sub> precursors. The photovoltaic properties were discussed in detail and were related to their charge separation processes and lifetime of CS state.

## 2. Experimental

### 2.1. Synthesis

Structures of the key compounds being synthesized and studied in this work are provided in Chart 1. While the other compounds were synthesized and studied previously [29,43–45], YD-TRC-NMF was first reported here and its synthetic routes were shown in Schemes 1 and 2. Other compounds discussed in this paper e.g. 4,4'-dimethyl-4''-styryl-triphenylamine (MTPA) [29] and 4-(4-methylphenyl)-7-styryl-1,2,3,3a,4,8b-hexahydrocyclopenta[b]indole (YD) [44] (ESI, Chart S1), D-A systems 4,4'-dimethyl-4''-(4-(4,6-dichloro-1,3,5-triazin-2-ylamino)styryl)triphenylamine (MTPA-TRC) [29] and 4-(4-methylphenyl)-7-(4-(4,6-dichloro-1,3,5-triazin-2-ylamino)styryl)-1,2,3,3a,4,8b-hexahydrocyclopenta[b]indole (YD-TRC) [43,44], D-A<sub>1</sub>-A<sub>2</sub> systems 4,4'-dimethyl-4''-(4-(4-chloro-6-(2-(9,10-dioxoanthracen-1-ylamino)ethylamino)-1,3,5-triazin-2-ylamino)styryl)triphenylamine (MTPA-TRC-AEAQ) [29], 4,4'-dimethyl-4''-(4-(4-Chloro-6-(N-(1-hexylheptyl)-N'-(4-amino)phenyl-perylene-3,4,9,10-tetracarboxylbisimide)-1,3,5-triazin-2-ylamino)styryl)triphenylamine (MTPA-TRC-PDI) [45], 4,4'-dimethyl-4''-(4-(4-Chloro-6-(N-(1-hexylheptyl)-N'-(4-amino)phenyl-1,7-di(4-*tert*-butylphenoxy)-perylene-3,4,9,10-tetracarboxylbisimide)-1,3,5-triazin-2-ylamino)styryl)triphenylamine (MTPA-TRC-PBI) [45] and 4-(4-methylphenyl)-7-(4-(4-chloro-6-(2-(9,10-dioxoanthracen-1-ylamino)ethylamino)-1,3,5-triazin-2-ylamino)styryl)-1,2,3,3a,4,8b-hexahydrocyclopenta[b]indole (YD-TRC-AEAQ) [44] were prepared according to the literature. The synthetic pathways of 4-(4-methylphenyl)-7-(4-(4-chloro-6-phenylamino-1,3,5-triazin-2-ylamino)styryl)-1,2,3,3a,4,8b-hexahydrocyclopenta[b]indole (YD-TRC-BA), *N*-methyl-2-(4-nitrophenyl)fulleropyrrolidine (NMF<sub>n</sub>), *N*-methyl-2-(4-aminophenyl)fulleropyrrolidine (NMF<sub>a</sub>), *N*-methyl-2-(4-(4,6-dichloro-1,3,5-triazin-2-ylamino)phenyl)fulleropyrrolidine (NMF<sub>t</sub>), 4-(4-methylphenyl)-7-(4-(4-chloro-6-(*N*-methyl-2-(4-phenyl)-fulleropyrrolidine)ylamino-1,3,5-triazin-2-ylamino)styryl)-1,2,3,3a,4,8b-hexahydrocyclopenta[b]indole (YD-TRC-NMF) were illustrated in Schemes 1 and 2. All reagents and solvents were reagent grade and further purified by the standard methods if necessary. All synthetic procedures were carried out under an atmosphere of dry nitrogen unless otherwise indicated.

### 2.2. Synthesis of YD-TRC-BA

YD-TRC (77.2 mg, 0.15 mmol) was dissolved in anhydrous THF (20 mL) and then phenylamine (14.0 mg, 0.15 mmol) was added into the solution. The mixture was stirred at 40 °C for 6 h. Afterwards, the solvent was removed by rotary evaporation and the residue was purified by column chromatography on silica gel using dichloromethane as the eluent. An orange solid was yielded (21.6 mg, 25.2%). HRMS-ESI (*m/z*): 571.2373 [M+H]<sup>+</sup> (calcd for C<sub>35</sub>H<sub>32</sub>ClN<sub>6</sub><sup>+</sup>: *m/z* = 571.2371). <sup>1</sup>HNMR (500 MHz, CDCl<sub>3</sub>): δ 7.55–7.47 (m, 7H), 7.34 (s, 1H), 7.18 (m, 7H), 7.03 (d, *J* = 16 Hz, 1H), 6.89 (dd, *J* = 16, 8.5 Hz, 2H), 4.81 (m, 1H), 3.85 (m, 1H), 2.35 (s, 3H), 2.12–1.49 (m, 6H). Elem. Anal.: Found: C, 73.52; H, 5.40; N, 14.84% (Calc. for C<sub>35</sub>H<sub>31</sub>ClN<sub>6</sub>: C, 73.61; H, 5.47; N, 14.72%)

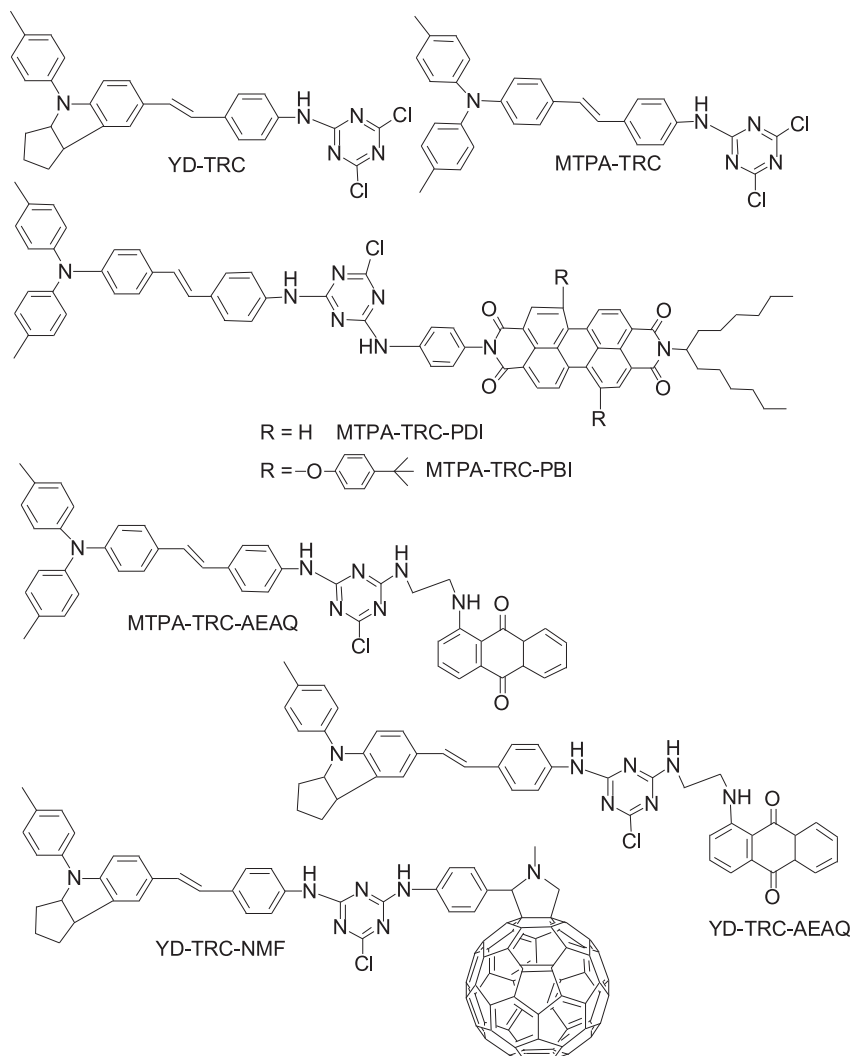
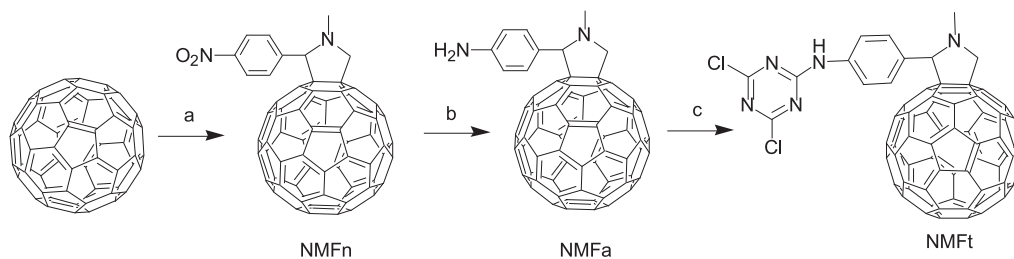


**Chart 1.** Structures of key compounds: MTPA-TRC, MTPA-TRC-AEAQ, MTPA-TRC-PDI, MTPA-TRC-PBI, YD-TRC, YD-TRC-AEAQ and YD-TRC-NMF.



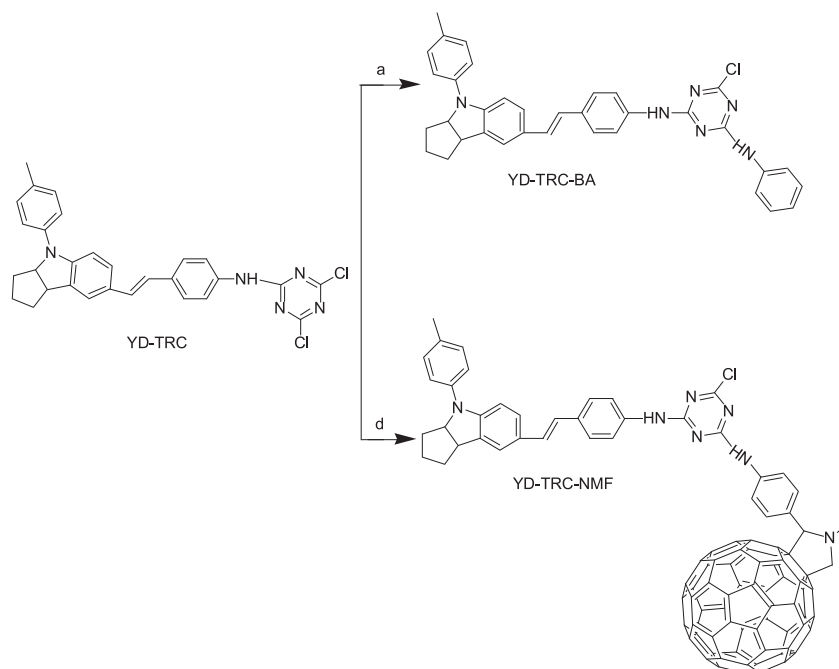
- a)  $N_2$ , *p*-nitrobenzaldehyde, sarcosine, 120 °C, 6h; b)  $N_2$ ,  $SnCl_2$ , concentrated HCl, 85 °C 1.5h; c)  $N_2$ , cyanuric chloride, 0 °C, 10 min.

**Scheme 1.** Synthesis scheme of NMFn, NMFa and NMFt.

### 2.3. Synthesis of NMFn

$C_{60}$  (240 mg, 0.33 mmol) was dissolved in the toluene (70 mL) and then *p*-nitrobenzaldehyde (53.5 mg, 0.35 mmol) and sarcosine (41.5 mg, 0.46 mmol) were added into the solution. The mixture was stirred at 120 °C for 6 h. Afterwards, the solvent was removed by rotary evaporation and the residue was purified by column

chromatography on silica gel using toluene as the eluent. A light brown solid was yielded (164 mg, 54.8%). MALDI-TOF-MS ( $m/z$ ): 898.07[M]<sup>+</sup> (calcd for  $C_{69}H_{10}N_2O_2$ :  $m/z = 898.0737$ ). <sup>1</sup>H NMR (500 MHz,  $C_7D_8$ ):  $\delta$  8.72 (d,  $J = 8.5$  Hz, 2H), 7.94 (d,  $J = 8.5$  Hz, 2H), 5.33 (s, 1H), 5.25 (d,  $J = 9.5$  Hz, 1H), 4.57 (d,  $J = 9.5$  Hz, 1H), 3.19 (s, 3H). Elem. Anal.: Found: C, 92.38; H, 1.21; N, 3.19% (Calc. for  $C_{69}H_{10}N_2O_2$ : C, 92.20; H, 1.12; N, 3.12%).



(a)  $N_2$ , phenylamine, 25 °C, 5min; (b)  $N_2$ , NMF, 80 °C, 24h.

**Scheme 2.** Synthesis scheme of YD-TRC-BA and YD-TRC-NMF.

#### 2.4. Synthesis of NMFa

NMFn (100 mg, 0.11 mmol) was dissolved in the toluene (45 mL) and ethanol (45 mL). The mixture was stirred at 25 °C for 1 h.  $SnCl_4 \cdot 2H_2O$  (124 mg, 0.55 mmol) and 2 mL concentrated HCl were added to the solution. The mixture was stirred at 50 °C for 7 h. Afterwards, the solvent was removed by rotary evaporation and the residue was purified by column chromatography on silica gel using toluene/dichloromethane (1:1 v/v) as the eluent. A light brown solid was yielded (164 mg, 54.8%). MALDI-TOF-MS ( $m/z$ ): 868.10[M]<sup>+</sup> (calcd for  $C_{69}H_{12}N_2^+$ :  $m/z = 868.0995$ ). <sup>1</sup>H NMR (500 MHz,  $CDCl_3/CS_2$ ):  $\delta$  7.33 (d,  $J = 8$  Hz, 2H), 6.68 (d,  $J = 8$  Hz, 2H), 4.83 (s, 2H), 4.29 (d,  $J = 6.5$  Hz, 1H), 4.25 (m, 1H), 4.07 (d,  $J = 6.5$  Hz, 1H), 2.81 (s, 3H).

#### 2.5. Synthesis of NMFt

Cyanuric chloride (18.3 g, 0.10 mmol) was first dissolved in anhydrous THF (20 mL) and then the solution was cooled down to 0 °C. NMFa (86.9 mg, 0.10 mmol) was added into the solution, followed by a stirring at 0 °C for 10 min. Then, the solution was warmed to room temperature while stirring for 30 min. Afterwards, the solvent was removed by rotary evaporation and the residue was purified by column chromatography on silica gel using petroleum toluene/dichloromethane (1:1 v/v) as the eluent to yield a yellow solid (0.21 g, 97.5%). MALDI-TOF-MS ( $m/z$ ): 1015.04[M]<sup>+</sup> (calcd for  $C_{72}H_{11}Cl_2N_5^+$ :  $m/z = 1015.0386$ ). <sup>1</sup>H NMR (500 MHz,  $CDCl_3/CS_2$ ):  $\delta$  9.43 (s, 1H), 7.61 (d,  $J = 8$  Hz, 2H), 7.44 (d,  $J = 8$  Hz, 2H), 4.29 (d,  $J = 6.5$  Hz, 1H), 4.25 (m, 1H), 4.07 (d,  $J = 6.5$  Hz, 1H), 2.81 (s, 3H).

#### 2.6. Synthesis of YD-TRC-NMF

YD-TRC (77.2 mg, 0.15 mmol) was dissolved in the anhydrous THF (20 mL) and then NMFa (130.3 mg, 0.15 mmol) were added into the solution. The mixture was stirred at 80 °C for 24 h.

Afterwards the solvent was removed by rotary evaporation and the residue was purified by column chromatography on silica gel using dichloromethane as the eluent. An olive-green solid was yielded (30.3 mg, 15%). MALDI-TOF-MS ( $m/z$ ): 1345.30[M]<sup>+</sup> (calcd for  $C_{98}H_{36}ClN_7^+$ :  $m/z = 1345.2715$ ). <sup>1</sup>H NMR (500 MHz,  $CDCl_3$ ):  $\delta$  7.56 (d,  $J = 8$  Hz, 3H), 7.35 (d,  $J = 8$  Hz, 2H), 7.28 (d,  $J = 8$  Hz, 3H), 7.16 (dd,  $J = 8.5, 8.5$  Hz, 6H), 7.10 (d,  $J = 8$  Hz, 2H), 6.98 (d,  $J = 16$  Hz, 1H), 6.84 (dd,  $J = 16, 8$  Hz, 2H), 5.07–4.89 (m, 3H), 4.76 (m, 1H), 3.79 (m, 1H), 2.83 (s, 3H), 2.33 (s, 3H), 2.11–1.73 (m, 6H).

#### 2.7. Assembly of single-layer organic solar cells

The single-layer organic solar cells were fabricated by placing MTPA-TRC, MTPA-TRC-AEAQ, MTPA-TRC-PDI, MTPA-TRC-PBI, YD-TRC, YD-TRC-AEAQ and YD-TRC-NMF in between FTO and Au electrodes. The FTO-coated glass substrate was first cleaned with detergent, ultrasonicated in water, washed with acetone and isopropyl alcohol, and then dried overnight in an oven at 50 °C under a vacuum of about  $3 \times 10^{-6}$  Torr. A film of MTPA-TRC (MTPA-TRC-AEAQ, MTPA-TRC-PDI, MTPA-TRC-PBI, YD-TRC, YD-TRC-AEAQ and YD-TRC-NMF) was prepared on the surface of FTO layer by spin coating from tetrahydrofuran solutions (10 mg/mL) and then a clean Au substrate of 45 nm was covered onto this film with vacuum evaporation. The fabricated solar cells were subsequently placed in a vacuum atmosphere of about  $3 \times 10^{-6}$  Torr for 3 h to remove the trace amounts of the solvent. All these procedures were carried out under an atmosphere of dry nitrogen. The active area of devices was 0.04 cm<sup>2</sup> and the thickness of the film was about 100 nm.

#### 2.8. Characterization

<sup>1</sup>H NMR, ESI mass and MALDI-TOF mass spectra were obtained on the VARIAN INOVA 500 MHz spectrometer, Thermo Fisher LCQ Deca XP MAX mass spectrometer and Bruker Autoflextof/tolIII mass

spectrometer, respectively. The testing temperature was set to 25 °C. The UV–vis absorption and fluorescence spectra were measured using a UV–vis spectrophotometer (ThermoSpectronic, Helios Gamma spectrometer) and a fluorescence spectrophotometer (Varian CARY ECLIPSE), respectively. Geometry optimizations, molecular orbitals and the corresponding energies of key compounds using B3LYP/6-31G(d,p) in toluene were carried out. The electrochemical properties were measured using a BAS 100 W electrochemical analyzer by cyclic voltammetry. Emission fluorescence decay spectra of the samples were done with picosecond diode lasers (Horiba Jobin Yvon Instruments) using Time-Correlated Single Photon Counting (TC-SPC). Nanosecond transient absorption measurements were performed on a LP-920 laser flash photolysis setup (Edinburgh). Some details of computations, cyclic voltammetry, emission fluorescence decay spectra and transient absorption spectra were exhibited in ESI. The current density-Voltage (J-V) characteristic of obtained solar cells was measured using solar simulator (Zolix) under AM 1.5 G (100 mW/cm<sup>2</sup>), which was adjusted using a calibrated Si solar cell (National Institute of Metrology), and recorded with a computer-controlled digital source meter (Kethly 2400).

### 3. Results and discussion

#### 3.1. Determination of YD-TRC-NMF as D-A<sub>1</sub>-A<sub>2</sub> architecture

To determine whether YD-TRC-NMF has a D-A<sub>1</sub>-A<sub>2</sub> architecture, cyclic voltammetry was used to measure the electrochemical curves of YD-TRC-NMF and its monomeric component parts. The electrochemical measurements are shown in Fig. S3 of ESI. For reported D-A system YD-TRC [44], there were one reversible oxidation wave ( $E_{1/2}^{0}$ , 0.28 V) ascribed to YD module and one irreversible reduction wave ( $E_{1/2}^{0}$ , -0.19 V) attributed to TRC module. Once NMF module has been attached to construct YD-TRC-NMF, the respective electrochemical curve shows one reversible oxidation wave and three reversible reduction waves (Fig. S3 of SI): The  $E_{1/2}^{0}$  (0.3 V) corresponds to the oxidation potential of YD module (0.28 V) while the  $E_{1/2}^{0}$ ,  $E_{1/2}^{2-}$  and  $E_{1/2}^{3-}$  (-0.93, -1.32 and -1.86 V) pertain to the reduction potentials of fullerene module NMFt (-0.92, -1.30 and -1.84 V). The reduction wave of TRC module in YD-TRC-NMF is covered by that of NMF module. Here we synthesized YD-TRC-BA so that the LUMO energy of TRC module can be evaluated by the reduction potential of YD-TRC-BA, and this method has been used in the reported D-A<sub>1</sub>-A<sub>2</sub> systems MTPA-TRC-AEAQ and YD-TRC-AEAQ [29,44].

As shown in Table 1, for YD-TRC-NMF, the HOMO and LUMO+1 levels are attributed to YD module, and HOMO-1 and LUMO levels pertain to NMF module, the LUMO level of TRC module is between that of YD module and NMF module in YD-TRC-NMF. The excited

electron in YD module can migrate to the TRC module followed by electron transfer to NMF module. Based on the experimental observation and computational results (Figs. S4–S5 of ESI), YD-TRC-NMF has a typical D-A<sub>1</sub>-A<sub>2</sub> architecture with cascade energy levels and should lead to the consecutive electron transfers. Additionally, the lower HOMO level of NMF module in comparison to that of YD module shows a possible hole transfer process from the excited NMF to YD module, thus making the triad ambipolar.

#### 3.2. YD-TRC-NMF as D-A<sub>1</sub>-A<sub>2</sub> architecture has the amazing long-lived CS state

As shown in Fig. 1, the absorption spectrum of the mixture of YD-TRC and NMFt is identical with the sum of the spectra of YD-TRC and NMFt, indicating that in the ground-state, the intermolecular non-bonded interactions between both modules are very weak. When a second acceptor NMF is attached to YD-TRC to form YD-TRC-NMF, the wavelength maxima (386 nm) of YD module is between those of YD (374 nm) and YD-TRC (402 nm), and the absorbance of NMF module is overlapped by that of YD module. This implies the existence of certain electronic and steric effects between both modules in YD-TRC-NMF, but these effects did not change the nature of various transitions as evidenced by similar shapes of the corresponding peaks.

The emission spectrum of the mixture of YD-TRC and NMFt is identical to the sum of the spectra of YD-TRC and NMFt (Fig. 2). The

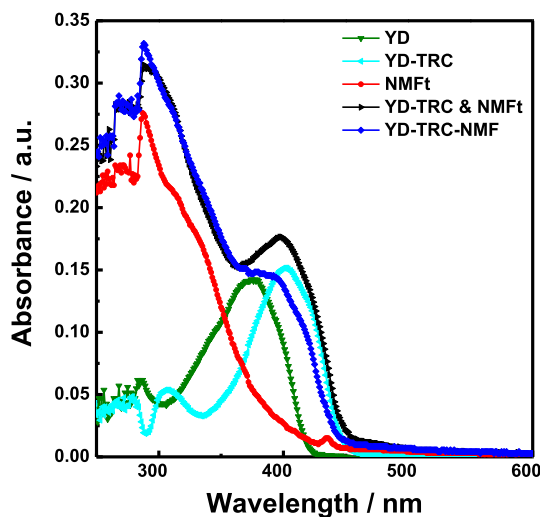


Fig. 1. Absorption of YD (olive), YD-TRC (cyan), NMFt (red), the equimolar mixture of YD-TRC and NMFt (black), and YD-TRC-NMF (blue) in toluene. (Concentration:  $5 \times 10^{-6}$  mol L<sup>-1</sup>). The data of YD and YD-TRC were taken from Ref. [44]. (For interpretation of the references to colour in this figure legend, the reader is referred to the web version of this article.)

Table 1  
Electrochemical data obtained vs Ag/Ag<sup>+</sup> in dichloromethane and frontier orbital energies.

Compounds	$E_{1/2}^{2/3-}$ <sup>a,b</sup> (V)	$E_{1/2}^{1-}$ <sup>a,b</sup> (V)	$E_{1/2}^{0}$ <sup>a,b</sup> (V)	$E_{1/2}^{0,b}$ (V)	$E_{\text{HOMO}}^c$ (eV)	$E_{\text{LUMO}}^c$ (eV)	$E_{\text{HOMO}-1}$ (eV)	$E_{\text{LUMO}+1}$ (eV)
YD <sup>a</sup>	–	–	–	0.24	-5.17	-2.53 <sup>e</sup>	–	–
YD-TRC <sup>a</sup>	–	–	-1.19	0.28	-5.21	-3.74	–	-2.65 <sup>e</sup>
NMFt	-1.84	-1.30	-0.92	–	-6.49 <sup>d</sup>	-4.01	–	–
YD-TRC-BA	–	–	-1.17	–	–	-3.76	–	–
YD-TRC-NMF	-1.86	-1.32	-0.93	0.30	-5.23	-4.00	-6.48 <sup>d</sup>	-2.67 <sup>e</sup>

<sup>a</sup> The data were taken from Ref. [44] for comparison purposes.

<sup>b</sup> V vs Ag/Ag<sup>+</sup>.

<sup>c</sup>  $E_{\text{HOMO}} = -E_{1/2}^{0} - 4.93$  eV;  $E_{\text{LUMO}} = -E_{1/2}^{0} - 4.93$  eV.

<sup>d</sup>  $E_{\text{HOMO}}(E_{\text{HOMO}-1}) = E_{\text{LUMO}} - E_{\text{gap}}^{\text{NMF}}$ , the optical band gap ( $E_{\text{gap}}^{\text{NMF}}$ , the value is 2.48 eV) was estimated from the onset of the absorption band of NMF module.

<sup>e</sup>  $E_{\text{LUMO}}(E_{\text{LUMO}+1}) = E_{\text{HOMO}} + E_{\text{gap}}^{\text{YD}}$ , the optical band gap ( $E_{\text{gap}}^{\text{YD}}$ , the values are 2.64 eV in compound YD, and 2.56 eV in compound YD-TRC and YD-TRC-NMF) was estimated from the onset of the ICT absorption band of YD module in toluene.

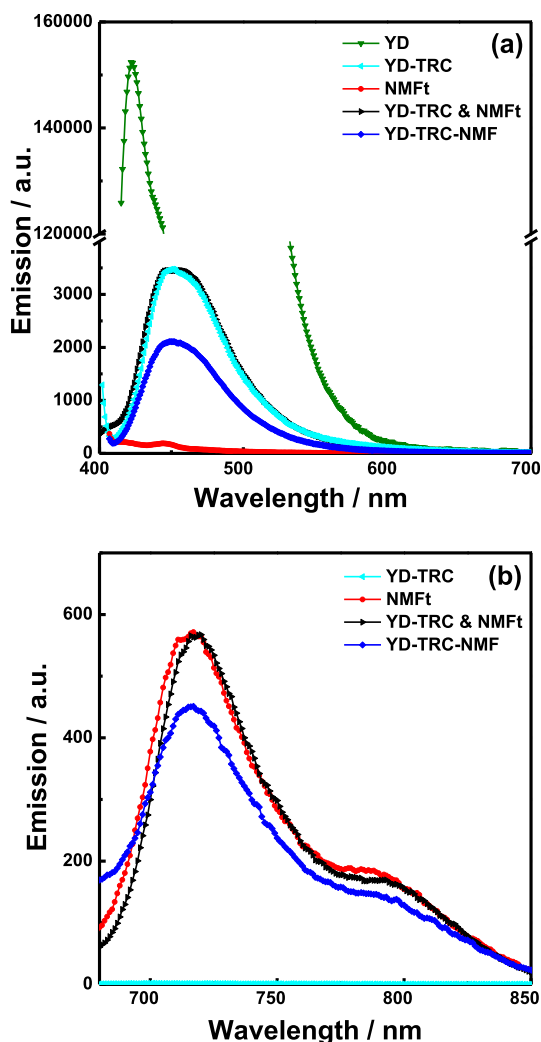


**Fig. 2.** Fluorescence emission spectra excited at 380 nm (a) and 470 nm (b) of YD (olive), YD-TRC (cyan), NMFt (red), the equimolar mixture of YD-TRC and NMFt (black), and YD-TRC-NMF (blue) in toluene (Concentration:  $5 \times 10^{-6}$  mol L $^{-1}$ ). (For interpretation of the references to colour in this figure legend, the reader is referred to the web version of this article.)

fluorescence from the mixture still follows a bi-exponential decay equation with similar lifetimes to those of pure YD-TRC and NMFt (Table 2 and Fig. S6 of ESI). This illustrates little change in the photophysical processes induced by the intermolecular interaction.

**Table 2**

Emission lifetimes and fractions (in parentheses) of YD, YD-TRC, NMFt, the equimolar mixture of YD-TRC and NMFt, and YD-TRC-NMF in toluene by fitting transient spectra with exponential decay equations.

Sample	Emission lifetime, $\tau$ /ns (fraction %)	
	$\lambda_{\text{ex}} = 366$ nm $\lambda_{\text{em}} = 460$ nm	$\lambda_{\text{ex}} = 457$ nm $\lambda_{\text{em}} = 717$ nm
YD <sup>a</sup>	1.26	–
YD-TRC <sup>a</sup>	0.82(66.8) 4.62(33.2)	–
NMFt	–	1.64
YD-TRC and NMFt	0.81(67.1) 4.65(32.9)	1.63
YD-TRC-NMF	1.02(74.1) 4.29(25.9)	0.36(75.5) 1.65(24.5)

<sup>a</sup> The data were taken from Ref. [44].

As shown in Fig. 2a, the emission intensity of YD module in YD-TRC and YD-TRC-NMF decreased by 96% and 98% respectively, compared to the reference compound YD when they are excited at 380 nm, where the YD module has a strong absorption but NMF module has a weak absorption. The fluorescence maximum from the YD module of YD-TRC-NMF (451 nm) is similar to that of YD-TRC (452 nm), but red-shifted from that of compound YD (422 nm). Meanwhile, the fluorescence of YD-TRC and YD-TRC-NMF at 460 nm follows the bi-exponential decay equation as shown in Table 2 and Fig. S6 of ESI. The fast decay components, which were measured as 0.82 ns for YD-TRC and 1.02 ns for YD-TRC-NMF, are assigned to the photo-induced electron transfer from YD to TRC module and consecutive electron transfer from YD to TRC module followed by an electron transfer to NMF module, respectively, whereas the slow decay component of YD-TRC-ABF (4.29 ns) is attributed to the salvation relaxation of YD singlet, and is clearly shorter than that in YD-TRC (4.62 ns). This is due to the intramolecular photoinduced Forster energy transfer which has been shown in similar D-TRC-A<sub>2</sub> systems [29,44], where the energy transfer is possible from the excited YD to the ABF module as the fluorescence emission spectrum of YD partially overlaps with the absorption spectrum of ABF.

When YD-TRC-NMF is excited at 470 nm (Fig. 2a), NMF module shows mild absorption, while little absorption was found for YD module. Therefore, only emissions from the NMF module were found for the triad and the fluorescence was quenched by about 42% with respect to the NMF module of compound NMFt. The fluorescence at 717 nm from NMF module decays bi-exponentially with lifetimes of 0.36 and 1.65 ns (Table 2 and Fig. S7 of SI). The fast component (0.36 ns) is attributed to the photo-induced hole transfer from the excited NMF to YD module to form the CS state YD<sup>+</sup>-TRC-NMF<sup>-</sup>, and the slow component (1.65 ns) is attributed to the singlet-triplet conversion, which is similar as the value of NMFt (1.64 ns).

To determine the lifetimes of the CS states in D-A<sub>1</sub> system YD-TRC and D-A<sub>1</sub>-A<sub>2</sub> system YD-TRC-NMF, nanosecond transient absorption measurements were performed. Fig. 3a shows the characteristics of YD<sup>+</sup> absorption of YD-TRC in the range 400–700 nm with the negative  $\Delta$ OD corresponding to the bleach of ground states [46–48]. Fig. 3b shows the formation of CS state YD<sup>+</sup>-TRC<sup>-</sup> with an estimated lifetime of 215 ns. [44]. When the second acceptor NMF is attached to YD-TRC, significantly different transient absorption spectra and kinetics of YD-TRC-NMF have been found. As shown in Fig. 3c, nanosecond transient absorption spectrum of YD-TRC-NMF reveals a wide peak in the 400 nm–600 nm range attributed to the YD<sup>+</sup> absorption and the peak at 710 nm corresponds to triplets <sup>3</sup>C<sub>60</sub><sup>\*</sup> absorption. However, the absorption of anions C60<sup>-</sup>, which was reported at 1020 nm is not observed in the spectra due to the instrument limitation [49,50]. The transient absorption at 710 nm follows a bi-exponential decay equation as shown in Fig. 3d, yielding two lifetimes of 7.9  $\mu$ s and 24.9  $\mu$ s indicating that there is overlap between YD<sup>+</sup> and <sup>3</sup>C<sub>60</sub><sup>\*</sup> absorption around 710 nm. The fast component (7.9  $\mu$ s) is attributed to YD<sup>+</sup> and is confirmed by the single-order decay equation of transient absorption at 550 nm, which remains unaffected by the introduction of the oxygen (Fig. S7 of ESI). The slow component (24.9  $\mu$ s) is ascribed to <sup>3</sup>C<sub>60</sub><sup>\*</sup>.

Thus, the 37-fold elongation of the lifetime of CS states in YD-TRC-NMF (7.9  $\mu$ s) over YD-TRC (215 ns) is determined in toluene, and the formation of outstandingly long-lived CS state of YD-TRC-NMF can be explained that the energy level of CS state was lower than that of acceptor2 (NMF) triplet state (Fig. 4). This principle has been shown in previous studies by others [51–57] ourselves [43,44]. Additionally, the reported D-A<sub>1</sub>-A<sub>2</sub> system YD-TRC-AEAQ also showed the consecutive electron transfer occurs from excited YD to TRC and then to AEAQ, resulting in a fivefold increase in the

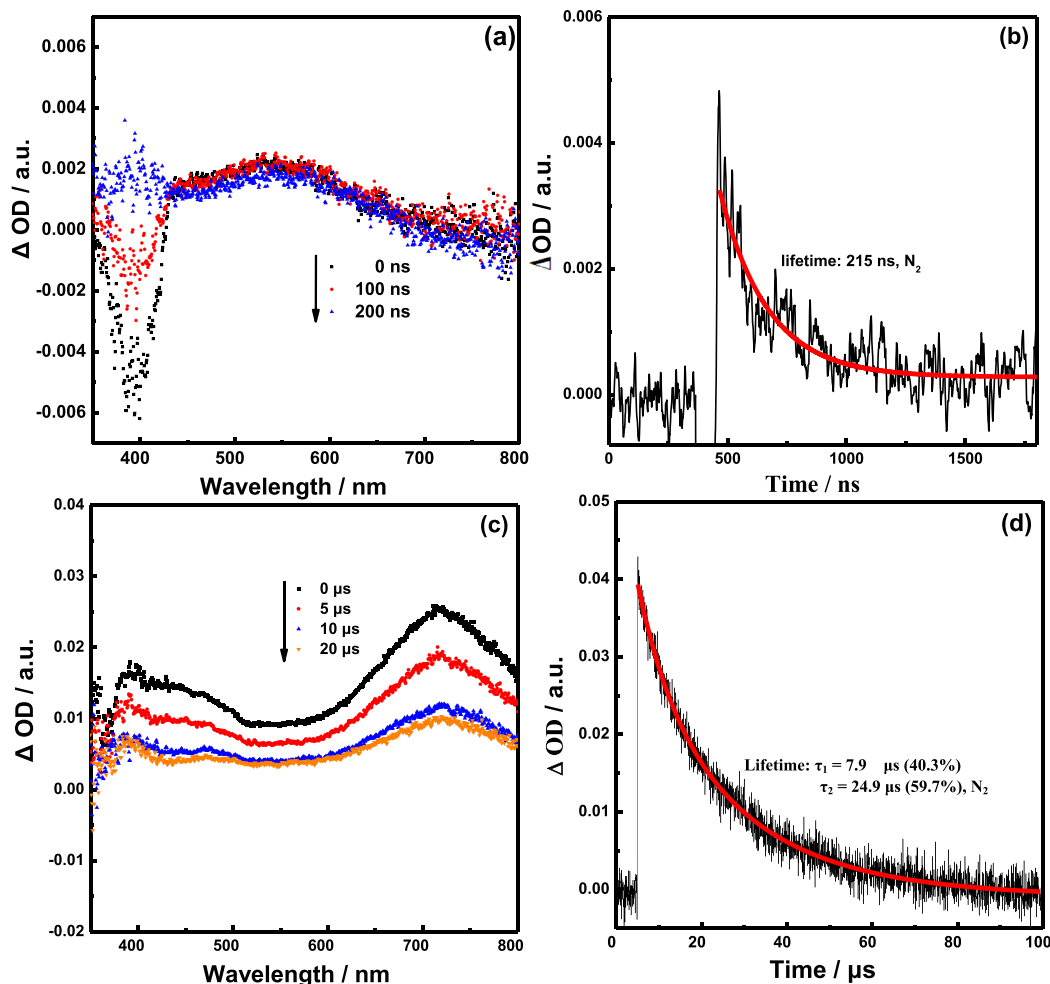


**Fig. 3.** Nanosecond transient absorption spectra (a) and kinetics at 540 nm (b) of YD-TRC and nanosecond transient absorption spectra (c) and kinetics at 710 nm (d) of YD-TRC-NMF in toluene following excitation with 410 nm, 8 ns laser pulses (Concentration:  $1 \times 10^{-5}$  mol L $^{-1}$ ). The red lines are the fitting curves by the single-order (b) and bi-exponential (d) exponential decay equation. The data of YD-TRC (a & b) was taken from Ref. [44]. (For interpretation of the references to colour in this figure legend, the reader is referred to the web version of this article.)

lifetime of charge separation of YD-TRC-AEAQ (1.14  $\mu$ s) in comparison with the same D-A $_1$  precursor YD-TRC (215 ns) [44]. This indicates that NMF as the acceptor should be more effective than AEAQ in forming the long-lived lifetime of CS states in D-A $_1$ -A $_2$  system. As shown in Fig. 4 a total of about 94% of excited YD singlets convert into the charge separated state in YD-TRC-ABF, indicating that D-A $_1$ -A $_2$  architecture through D-A $_1$  precursor can be used as an important design principle to achieve CS states effectively.

### 3.3. Using long-lived CS states to improve efficiency of single layer organic solar cells with D-A $_1$ -A $_2$ architected materials

Using TRC as an acceptor, we have obtained two D-A type organic semiconductors, MTPA-TRC and YD-TRC, and five D-A $_1$ -A $_2$  type ambipolar organic semiconductors, MTPA-TRC-PDI, MPA-TRC-PBI, MTPA-TRC-AEAQ, YD-TRC-AEAQ and YD-TRC-NMF. Here, we have employed these dyes to assemble single layer organic solar cells, FTO/Dye/Au. Consecutive photo-induced electron transfer occurred from D to TRC to A $_2$  and then to FTO, and photo-induced hole transfer occurred from A $_2$  to D directly and then to Au, which is allowed in these devices because LUMO of A $_2$  is higher than the conduction band of FTO (−4.4 eV) and HOMO of D is lower

than the work function of Au (−5.1 eV) (Table S1 of ESI). Fig. 5 shows device structure and the current density-voltage (J-V) curves of the seven compounds in these solar cells under AM 1.5 G illumination. The photovoltaic performances in cells and overall generation efficiency from excited donor singlets and lifetimes of CS states in toluene of corresponding compounds are given in Table 3.

For ambipolar organic semiconductors, we could not detect any photocurrents with devices of MTPA-TRC-PDI, and MTPA-TRC-PBI exhibits a very low short circuit current  $J_{sc}$  and power conversion efficiency  $\eta$  similar to MTPA-TRC. These correspond to their relatively short lifetime of CS states due to efficient conversions from the CS states MTPA $^{+}$ -TRC-PDI $^{-}$  and MTPA $^{+}$ -TRC-PBI $^{-}$  to the triplet states MTPA-TRC- $^3$ PDI $^*$  and MTPA-TRC- $^3$ PBI $^*$ , respectively [45]. Intriguingly, device of MTPA-TRC-AEAQ shows a clearly increased  $J_{sc}$  and  $\eta$ , agreeing well with its 8-time-longer lifetime of CS states, in comparison with those of MTPA-TRC. This suggests that the longer lifetime of CS states for the dyes benefits their photovoltaic performance.

As the donor was replaced by YD module, YD-TRC presented similarly low photovoltaic characteristics as observed in MTPA-TRC, yet its lifetime of CS states was extended to 215 ns, about 2.5 times

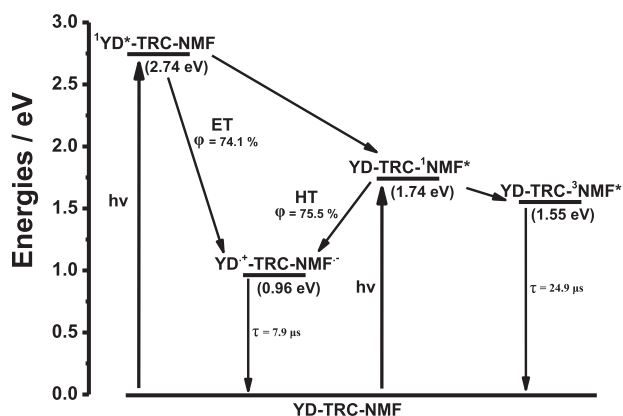


**Fig. 4.** Energy level diagram and photophysical processes of YD-TRC-NMF upon excitation in toluene with singlet energies of various compounds from the fluorescence spectra and the triplet energies of NMF from literature data [49]. The energy of charge separated state  $\text{YD}^{+\bullet}\text{-TRC-NMF}^{-\bullet}$  ( $-\Delta G_{\text{CR}}$ ) was estimated by the equation  $-\Delta G_{\text{CR}} = e(E_{\text{ox}} - E_{\text{red}})$ , and  $E_{\text{ox}}$  is the first one-electron oxidation potential of the donor (YD) module, while  $E_{\text{red}}$  refers to the first one-electron reduction potential of the acceptor2 (NMF) module.

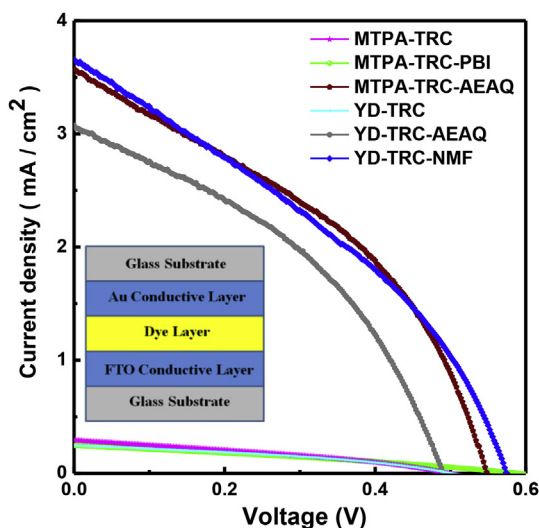


**Fig. 5.** Device structure and J-V curves of obtained single layer organic photovoltaic cells FTO/Dye/Au based on MTPA-TRC (magenta), MTPA-TRC-PBI (green), MTPA-TRC-AEAQ (wine), YD-TRC (cyan), YD-TRC-AEAQ (gray) and YD-TRC-NMF (blue). (For interpretation of the references to colour in this figure legend, the reader is referred to the web version of this article.)

**Table 3**

Photovoltaic performances of single layer organic photovoltaic cells FTO/Dye/Au under AM 1.5 G illumination, and overall generation efficiency ( $\phi$ ) from excited donor singlets and lifetimes ( $\tau$ ) of CS states of respective dyes in toluene.

Dyes	$V_{\text{oc}}/\text{V}$	$J_{\text{sc}}/\text{mA}/\text{cm}^2$	FF/%	$\eta/\%$	$\phi/\%^a$	$\tau/\text{ns}^a$
MTPA-TRC	0.50	0.29	32.6	0.04	40	80
MTPA-TRC-PDI	—	—	—	—	—	—
MTPA-TRC-PBI	0.59	0.25	30.0	0.04	77	75
MTPA-TRC-AEAQ	0.55	3.59	39.0	0.77	84	650
YD-TRC	0.50	0.25	36.5	0.04	67	215
YD-TRC-AEAQ	0.49	3.08	39.7	0.60	98	1140
YD-TRC-NMF	0.57	3.68	34.6	0.73	94	7900

<sup>a</sup> The data except YD-TRC-NMF were taken from Refs. [44,45].

than that of MTPA-TRC. The photovoltaic characteristics ( $J_{\text{sc}}$  and  $\eta$ ) are significantly improved in devices of YD-TRC-AEAQ and YD-TRC-NMF. The  $J_{\text{sc}}$  and  $\eta$  are clearly higher with YD-TRC-NMF than YD-TRC-AEAQ, though the absorption ability in visible light and overall generation efficiency from excited YD singlets of CS states (Table S1 of ESI and Table 3) for YD-TRC-AEAQ, which are higher than those for YD-TRC-NMF. This could be explained by the longer CS states in YD-TRC-NMF.

However, although the lifetime of CS states has been prolonged to 1.14  $\mu\text{s}$ , YD-TRC-AEAQ shows a relatively low  $J_{\text{sc}}$  and  $\eta$  than MTPA-TRC-AEAQ. Only YD-TRC-NMF with a CS state lifetime of 7.9  $\mu\text{s}$  shows comparable photovoltaic properties with MTPA-TRC-AEAQ. This may be due to the lower visible light absorption ability of YD module when compared to the MTPA module, as well as the fact that the visible light absorption of the second acceptor in YD-TRC-AEAQ or YD-TRC-ABF is clearly lower than that in MTPA-TRC-AEAQ (Table S1 of ESI). The results from Table 3 indicate that, as the  $J_{\text{sc}}$  is below 3  $\text{mA}/\text{cm}^2$ , the  $J_{\text{sc}}$  and  $\eta$  may increase obviously and couple with the improvement of CS state lifetime of ambipolar organic semiconductors, revealing a positive effect of long-lived CS states. However, when the  $J_{\text{sc}}$  is beyond 3  $\text{mA}/\text{cm}^2$ , the elongated lifetime of CS states yield a limited effect on the photovoltaic performance of single layer organic solar cells. This means that the charge transfer at the interfaces between organic semiconductors and inorganic electrode significantly influences the formation of currents. Moreover, The far better photovoltaic characteristics of D-TRC-A<sub>2</sub> than D-TRC suggests potential applications in OSCs, if better structural designing of OSCs and extension of absorption spectrum range of organic optoelectronic material.

#### 4. Conclusions

In this paper, we have synthesized and characterized a new D-A<sub>1</sub>-A<sub>2</sub> system: YD-TRC-NMF. Sequential electron transfers from excited YD to TRC then to NMF module and the hole transfer from the excited NMF to YD module were revealed in YD-TRC-NMF upon light absorption.

The lifetime of CS state of YD-TRC-NMF is 7.9  $\mu\text{s}$ , a 37-fold elongation over YD-TRC as 215 ns. The formation of outstandingly long-lived CS state of YD-TRC-NMF was explained by noting that the energy level of CS state was lower than that of acceptor2 (NMF) triplet state. This result absolutely confirms the rationale behind using D-A<sub>1</sub>-A<sub>2</sub> architecture via D-A<sub>1</sub> precursor to obtain the long-lived CS state.

The photovoltaic tests indicate potential applications of YD-TRC-NMF (or AEAQ) and MTPA-TRC-AEAQ in solar cells. In these D-TRC-A<sub>2</sub> systems, the triplet states of acceptor2 are higher than CS states, and the photovoltaic characteristics ( $J_{\text{sc}}$  and  $\eta$ ) are significantly improved in comparison with those of their D-TRC precursors. Long-lived CS states can play an important role in promoting photoelectric conversion in devices of D-A<sub>1</sub>-A<sub>2</sub> architected photovoltaic materials. However, the positive effect of CS states will be limited as the interfacial charge transfer between organic semiconductors and inorganic electrode, which is the ultimate factor that determines device performance. This sheds a light on the design of novel D-A<sub>1</sub>-A<sub>2</sub> architectures for organic photovoltaics and other optoelectronic device.

#### Acknowledgments

This work was supported by the National Nature Science Foundation of China (Grant No. 21576195 and 21506151) and Tianjin science and technology innovation platform program (No. 14TXGCCX00017). Lichang Wang acknowledges the support by the Tianjin 1000 talent program for her stay at Tianjin University.

## Appendix A. Supplementary data

Supplementary data related to this article can be found at <http://dx.doi.org/10.1016/j.dyepig.2016.12.066>.

## References

- [1] McConnell I, Li G, Brudvig GW. Energy conversion in natural and artificial photosynthesis. *Chem Biol* 2010;17(5):434–47.
- [2] Cowan AJ, Durrant JR. Long-lived charge separated states in nanostructured semiconductor photoelectrodes for the production of solar fuels. *Chem Soc Rev* 2013;42(6):2281–93.
- [3] Kodis G, Liddell PA, de la Garza L, Clausen PC, Lindsey JS, Moore AL, et al. Efficient energy transfer and electron transfer in an artificial photosynthetic antenna-reaction center complex. *J Phys Chem A* 2002;106(10):2036–48.
- [4] Kashiwagi Y, Ohkubo K, McDonald JA, Blake IM, Crossley MJ, Araki Y, et al. Long-lived charge-separated state produced by photoinduced electron transfer in a zinc imidazopyrroline-C60 dyad. *Org Lett* 2003;5(15):2719–21.
- [5] Guldi DM, Imahori H, Tamaki K, Kashiwagi Y, Yamada H, Sakata Y, et al. A molecular tetrad allowing efficient energy storage for 1.6 s at 163 K. *J Phys Chem A* 2004;108(4):541–8.
- [6] Fukuzumi S, Saito K, Ohkubo K, Khoury T, Kashiwagi Y, Absalom MA, et al. Multiple photosynthetic reaction centres composed of supramolecular assemblies of zinc porphyrin dendrimers with a fullerene acceptor. *Chem Comm* 2011;47(28):7980–2.
- [7] Imahori H, Guldi DM, Tamaki K, Yoshida Y, Luo C, Sakata Y, et al. Charge separation in a novel artificial photosynthetic reaction center lives 380 ms. *J Am Chem Soc* 2001;123(27):6617–28.
- [8] Kawashima Y, Ohkubo K, Kentaro M, Fukuzumi S. Electron transfer in a supramolecular complex of zinc chlorin carboxylate anion with Li<sup>+</sup>@C60 affording the long-lived charge-separated state. *J Phys Chem C* 2013;117(41):21166–77.
- [9] Fukuzumi S, Itoh A, Suenobu T, Ohkubo K. Formation of the long-lived charge-separated state of the 9-Mesityl-10-methylacridinium cation incorporated into mesoporous aluminosilicate at high temperatures. *J Phys Chem C* 2014;118(41):24188–96.
- [10] Bottari G, de la Torre G, Guldi DM, Torres T. Covalent and noncovalent phthalocyanine–carbon nanostructure systems: synthesis, photoinduced electron transfer, and application to molecular photovoltaics. *Chem Rev* 2010;110(11):6768–816.
- [11] Petrus ML, Morgenstern FS, Sadhanala A, Friend RH, Greenham NC, Dingemans TJ. Device performance of small-molecule azomethine-based bulk heterojunction solar cells. *Chem Mater* 2015;27(8):2990–7.
- [12] Mishra A, Bäuerle P. Small molecule organic semiconductors on the move: promises for future solar energy technology. *Angew Chem Int Ed* 2012;51(9):2020–67.
- [13] Loi MA, Denk P, Hoppe H, Neugebauer H, Winder C, Meissner D, et al. Long-lived photoinduced charge separation for solar cell applications in phthalocyanine–fulleropyrroline dyad thin films. *J Mater Chem* 2003;13(4):700–4.
- [14] Alsulami QA, Murali B, Alsinan Y, Parida MR, Aly SM, Mohammed OF. Remarkably high conversion efficiency of inverted bulk heterojunction solar cells: from ultrafast laser spectroscopy and electron microscopy to device fabrication and optimization. *Adv Energy Mater* 2016;6(11):1502356.
- [15] Ohkubo K, Kawashima Y, Sakai H, Hasobe T, Fukuzumi S. Enhanced photoelectrochemical performance of composite photovoltaic cells of Li<sup>+</sup>@C60-sulphonated porphyrin supramolecular nanoclusters. *Chem Comm* 2013;49(40):4474–6.
- [16] Ohkubo K, Kawashima Y, Fukuzumi S. Strong supramolecular binding of Li<sup>+</sup>@C60 with sulfonated meso-tetraphenylporphyrins and long-lived photoinduced charge separation. *Chem Comm* 2012;48(36):4314–6.
- [17] Blanco GD, Hiltunen AJ, Lim GN, Kc CB, Kaunisto K, Vuorinen T, et al. Syntheses, charge separation and inverted bulk heterojunction solar cell application of phenothiazine–fullerene dyads. *ACS Appl Mater Interfaces* 2016;8:8481–90.
- [18] Rao KP, Kusamoto T, Toshimitsu F, Inayoshi K, Kume S, Sakamoto R, et al. Double protonation of 1, 5-bis (triarylaminoethyl) anthraquinone to form a paramagnetic pentacyclic dipyrilium salt. *J Am Chem Soc* 2010;132(35):12472–9.
- [19] Lemaire V, Steel M, Beljonne D, Brédas J-L, Cornil J. Photoinduced charge generation and recombination dynamics in model donor/acceptor pairs for organic solar cell applications: a full quantum-chemical treatment. *J Am Chem Soc* 2005;127(16):6077–86.
- [20] Kwon T-H, Armel V, Nattestad A, MacFarlane DR, Bach U, Lind SJ, et al. Dithienothiophene (DTT)-based dyes for dye-sensitized solar cells: synthesis of 2, 6-dibromo-DTT. *J Org Chem* 2011;76(10):4088–93.
- [21] Gupta G, Singh CR, Lohwasser RH, Himmerlich M, Krischok S, Mueller-Buschbaum P, et al. Morphology, crystal structure and charge transport in donor-acceptor block copolymer thin films. *ACS Appl Mater Interfaces* 2015;7(23):12309–18.
- [22] Punireddi SR, Kiersnowski A, Battagliarin G, Zajackowski W, Wong WWH, Kirby N, et al. Polythiophene-terylene diimide heterojunction field-effect transistors. *J Mater Chem C* 2013;1(13):2433–40.
- [23] Varathan E, Vijay D, Subramanian V. Rational design of carbazole- and carboline-based ambipolar host materials for blue electrophosphorescence: a density functional theory study. *J Phys Chem C* 2014;118(38):21741–54.
- [24] Feng X, Chen L, Honsho Y, Saengsawang O, Liu L, Wang L, et al. An ambipolar conducting covalent organic framework with self-sorted and periodic electron donor-acceptor ordering. *Adv Mater* 2012;24(22):3026–31.
- [25] Usta H, Newman C, Chen Z, Facchetti A. Dithienocoronediimide-based copolymers as novel ambipolar semiconductors for organic thin-film transistors. *Adv Mater* 2012;24(27):3678–84.
- [26] Magnuson A, Anderlund M, Johansson O, Lindblad P, Lomoth R, Polivka T, et al. Biomimetic and microbial approaches to solar fuel generation. *Acc Chem Res* 2009;42(12):1899–909.
- [27] Poddutoori PK, Zarrabi N, Moiseev AG, Gumbau-Brisa R, Vassiliev S, van der Est A. Long-lived charge separation in novel axial donor–porphyrin–acceptor triads based on tetrathiafulvalene, aluminum (III) porphyrin and naphthalenediimide. *Chem Eur J* 2013;19(9):3148–61.
- [28] Supur M, El-Khouly ME, Seok JH, Kay K-Y, Fukuzumi S. Elongation of lifetime of the charge-separated state of ferrocene–naphthalenediimide–[60] fullerene triad via stepwise electron transfer. *J Phys Chem A* 2011;115(50):14430–7.
- [29] Wang T, Weerasinghe KC, Liu D, Li W, Yan X, Zhou X, et al. Ambipolar organic semiconductors with cascades of energy levels for generating long-lived charge separated states: a donor–acceptor1–acceptor2 architectural triarylamine dye. *J Mater Chem C* 2014;2(28):5466–70.
- [30] Wang T, Sun H, Lu T, Bridgman CN, Li F, Liu D, et al. Dissociation exists in s-triazine based donor-acceptor organic systems by photo-induced electron transfer. *Dyes Pigm* 2017;139:264–73.
- [31] Antohe S. Electrical and photoelectrical properties of the single-, and multi-layer organic photovoltaic cells. *J Optoelectron Adv Mater* 2000;2(5):498–514.
- [32] Ghosh AK, Morel DL, Feng T, Shaw RF, Rowe Jr CA. Photovoltaic and rectification properties of Al/Mg phthalocyanine/Ag Schottky-barrier cells. *J Appl Phys* 1974;45(1):230–6.
- [33] Karg S, Riess W, Dyakonov V, Schwoerer M. Electrical and optical characterization of poly (phenylene-vinylene) light emitting diodes. *Synth Met* 1993;54(1–3):427–33.
- [34] Cnops K, Rand BP, Cheyng D, Verreert B, Empl MA, Heremans P. 8.4% efficient fullerene-free organic solar cells exploiting long-range exciton energy transfer. *Nat Commun* 2014;5.
- [35] Saeki A, Tsuji M, Yoshikawa S, Gopal A, Seki S. Boosting photovoltaic performance of a benzobisthiazole based copolymer: a device approach using a zinc oxide electron transport layer. *J Mater Chem A* 2014;2(17):6075–80.
- [36] You J, Dou L, Yoshimura K, Kato T, Ohya K, Moriarty T, et al. A polymer tandem solar cell with 10.6% power conversion efficiency. *Nat Commun* 2013;4:1446.
- [37] Zhou H, Yang L, Stuart AC, Price SC, Liu S, You W. Development of fluorinated benzothiadiazole as a structural unit for a polymer solar cell of 7% efficiency. *Angew Chem Int Ed* 2011;123(13):3051–4.
- [38] Chen TL, Zhang Y, Smith P, Tamayo A, Liu Y, Ma B. Diketopyrrolopyrrole-containing oligothiophene–fullerene triads and their use in organic solar cells. *ACS Appl Mater Interfaces* 2011;3(7):2275–80.
- [39] Narayanaswamy K, Venkateswararao A, Nagarjuna P, Bishnoi S, Gupta V, Chand S, et al. An organic dyad composed of diathiafulvalene-functionalized diketopyrrolopyrrole–fullerene for single-component high-efficiency organic solar cells. *Angew Chem Int Ed* 2016;55(40):12334–7.
- [40] Nierengarten JF, Eckert JF, Nicoud JF, Ouali L, Krasnikov V, Hadziioannou G. ChemInform abstract: synthesis of a C60-oligothiophenevinylene hybrid and its incorporation in a photovoltaic device. *Chem Comm* 1999;30(28):617–8.
- [41] Izawa S, Hashimoto K, Tajima K. Efficient charge generation and collection in organic solar cells based on low band gap dyad molecules. *Chem Comm* 2011;47(22):6365–7.
- [42] Cao J, Du X, Chen S, Xiao Z, Ding L. A dumbbell-like A-D-A molecule for single-component organic solar cells. *Phys Chem Chem Phys* 2014;16(8):3512–4.
- [43] Lu T, Sun H, Colley ND, Bridgman CN, Liu D, Li W, et al. Tuning the donors to control the lifetimes of charge separated states in triazine-based donor-acceptor systems. *Dyes Pigm* 2017;136:404–15.
- [44] Wang T, Zhao C, Zhang L, Lu T, Sun H, Weerasinghe KC, et al. Enhancing photoinduced charge separation through donor moiety in donor-acceptor organic semiconductors. *J Phys Chem C* 2016;120(44):25263–75.
- [45] Wang T, Weerasinghe KC, Sun H, Hu X, Lu T, Liu D, et al. Effect of triplet state on the lifetime of charge separation in ambipolar d-a1-a2 organic semiconductors. *J Phys Chem C* 2016;120(21):11338–49.
- [46] Burdzinski G, Karolczak J, Ziótek M. Dynamics of local Stark effect observed for a complete D149 dye-sensitized solar cell. *Phys Chem Chem Phys* 2013;15(11):3889–96.
- [47] El-Zohry AM, Roca-Sanjuan D, Ziet B. Ultrafast twisting of the indoline donor unit utilized in solar cell dyes: experimental and theoretical studies. *J Phys Chem C* 2015;119(5):2249–59.
- [48] Sobuś J, Karolczak J, Komar D, Anta JA, Ziótek M. Transient states and the role of excited state self-quenching of indoline dyes in complete dye-sensitized solar cells. *Dyes Pigm* 2015;113:692–701.
- [49] Bandi V, Gobeze HB, D'Souza F. Ultrafast photoinduced electron transfer and charge stabilization in donor–acceptor dyads capable of harvesting near-infrared light. *Chem Eur J* 2015;21(32):11483–94.
- [50] Bandi V, Gobeze HB, Lakshmi V, Ravikanth M, D'Souza F. Vectorial charge separation and selective triplet-state formation during charge recombination in a pyrrolyl-bridged BODIPY–fullerene dyad. *J Phys Chem C* 2015;119(15):

- 8095–102.
- [51] Blas-Ferrando VM, Ortiz J, Bouissane L, Ohkubo K, Fukuzumi S, Fernandez-Lazaro F, et al. Rational design of a phthalocyanine-perylene diimide dyad with a long-lived charge-separated state. *Chem Comm* 2012;48(50):6241–3.
- [52] Das SK, Song B, Mahler A, Nesterov VN, Wilson AK, Ito O, et al. Electron transfer studies of high potential zinc porphyrin-fullerene supramolecular dyads. *J Phys Chem C* 2014;118(8):3994–4006.
- [53] Liu J-Y, El-Khouly ME, Fukuzumi S, Ng DKP. Photoinduced electron transfer in a distyryl BODIPY-fullerene dyad. *Chem Asian J* 2011;6(1):174–9.
- [54] Robotham B, Lastman KA, Langford SJ, Ghiggino KP. Ultrafast electron transfer in a porphyrin-amino naphthalene diimide dyad. *J Photochem Photobiol A* 2013;251:167–74.
- [55] Fukuzumi S, Ohkubo K. Long-lived photoinduced charge separation for solar cell applications in supramolecular complexes of multi-metalloporphyrins and fullerenes. *Dalton Trans* 2013;42(45):15846–58.
- [56] Tanaka M, Ohkubo K, Gros CP, Guillard R, Fukuzumi S. Persistent electron-transfer state of a  $\pi$ -complex of acridinium ion inserted between porphyrin rings of cofacial bisporphyrins. *J Am Chem Soc* 2006;128(45):14625–33.
- [57] Veldkamp BS, Han W-S, Dyar SM, Eaton SW, Ratner MA, Wasielewski MR. Photoinitiated multi-step charge separation and ultrafast charge transfer induced dissociation in a pyridyl-linked photosensitizer-cobaloxime assembly. *Energy Environ Sci* 2013;6(6):1917–28.